

Contents lists available at ScienceDirect

Journal of Magnetic Resonance

journal homepage: www.elsevier.com/locate/jmr



Silicon-29 echo train coherence lifetimes and geminal ²*J*-couplings in network modified silicate glasses



Daniel Jardón-Álvarez, Mark O. Bovee, Philip J. Grandinetti*

Department of Chemistry, The Ohio State University, 120 W. 18th Avenue, Columbus, OH 43210-1173, USA

ARTICLE INFO

Article history: Received 30 September 2021 Revised 25 October 2021 Accepted 25 October 2021 Available online 28 October 2021

Keywords:
²⁹Si solid state NMR
Transverse relaxation
J couplings
Homogeneous broadening mechanisms
Silicate glasses

ABSTRACT

The natural abundance ²⁹Si echo-train coherence lifetimes in network-modified silicate glasses were examined under static and magic-angle spinning (MAS) conditions. The nuclear magnetic properties of modifier cations were found to play a major role in determining ²⁹Si coherence lifetimes, leading to differences as large as three orders of magnitude. In compositions with abundant NMR active nuclei, such as alkali silicates, the ²⁹Si coherence lifetimes are dominated by coherent dephasing due to residual heteronuclear dipolar couplings, whereas in compositions dilute in NMR active nuclei, such as alkaline earth silicates, the ²⁹Si coherence lifetimes are dominated by incoherent dephasing due to paramagnetic impurities. Expressing the inverse of the coherence lifetime as a residual full width at half maximum (FWHM), we found that increasing rates of both MAS and a π -pulse train are effective in removing the residual ²⁹Si heteronuclear broadenings, with a near-linear relationship between FWHM and MAS rotor period and π -pulse spacing. Based on these results, we conclude that accurate 29 Si J coupling measurements will be the most challenging in lithium silicate glasses due to strong homonuclear dipolar couplings among ⁷Li nuclei, requiring MAS speeds up to 100 kHz, and be the least challenging in the alkaline earth silicate glasses. At a modest MAS speed of 14 kHz, distributions of geminal I couplings across Si-O-Si linkages were measured in alkali and alkaline earth silicate glasses giving mean values of 4.2 Hz and 5.1 Hz in 0.4 CaO·0.6 SiO₂ and 0.33 Ba₂O·0.67 SiO₂ glasses, respectively, and 5.2 Hz and 5.3 Hz in 0.33 $Na_2O.0.67 SiO_2$ and 0.33 $K_2O.0.67 SiO_2$ glasses, respectively. We also observe greater variance in the I distributions of alkaline earth silicate glasses consistent with greater structural disorder due to increased modifier cation potential, i.e., the charge-to-radius ratio, \mathbb{Z}/r of the cation.

© 2021 Elsevier Inc. All rights reserved.

1. Introduction

Silicon-29 nuclear magnetic resonance (NMR) spectroscopy is a powerful experimental method for obtaining insight on the atomic-level structure of silicate glasses. Distributions in nuclear spin interaction parameters, such as isotropic chemical shifts, chemical shift anisotropies and J couplings, can be mapped to relevant structural distributions in Q^n species, bond lengths, and angles [1–4]. In such measurements, long coherence lifetimes are essential for accurate frequency measurements, particularly for determining ²⁹Si geminal J couplings, which are on the order of 1–20 Hz in silicates [5], requiring $\Lambda \ll J$, where Λ is the residual full-width at half maximum after a combined coherent averaging with magic-angle spinning (MAS) and a π -pulse train. Additionally, extended echo-train coherence lifetimes can provide dramatic sen-

E-mail addresses: daniel.jardon-alvarez@weizmann.ac.il (D. Jardón-Álvarez), bovee.4@osu.edu (M.O. Bovee), grandinetti.1@osu.edu (P.J. Grandinetti).

sitivity enhancements with echo-train acquisition of the spectra with strong inhomogeneous line broadenings, such as glasses, and half-integer quadrupolar nuclei with strong second-order broadenings [6–10].

The coherence lifetimes under MAS and a π -pulse train are often governed by the secular part of some relaxation mechanism [11] or a coherent dephasing due to residual heteronuclear dipolar couplings to a spin bath of dipolar coupled homonuclear spins [12]. Both contributions can be reduced or eliminated and coherence lifetimes lengthened by increasing the MAS spinning rate, the π -pulse rate, or both. In terms of relaxation theory, the MAS spinning or π -pulse train rate gets introduced into the spectral densities in a manner akin to the Larmor and Rabi frequencies [11]. While this will be negligible in the case of longitudinal relaxation, it can strongly affect transverse relaxation caused by slow fluctuations [13]. A. J. Vega [14] showed that the T_2 dependence on the correlation time of a fluctuating Hamiltonian, τ_c , inverts when the coherent averaging period, τ_p , becomes smaller than τ_c . Therefore, for slow motions and under an appropriate coherent averaging

^{*} Corresponding author.

scheme, T_2 is not locked at the rigid lattice limit but passes through a minimum and grows with shorter τ_c values according to

$$\frac{1}{T_2} \sim \delta^2 \tau_p^2 / \tau_c,\tag{1}$$

where δ is the magnitude of the fluctuating Hamiltonian.

In this paper, we (a) examine the mechanisms responsible for 29 Si π -pulse echo train coherence lifetimes in a series of alkali and alkaline earth silicate glasses under static and magic-angle spinning conditions, (b) determine how decay constants associated with these processes are related to local structure and dynamics, and (c) develop strategies for lengthening coherence lifetimes to enable accurate and precise measure of geminal J couplings between 29 Si nuclei across the Si-O-Si linkage [2,5,15] in network modified silicate glasses.

In these efforts, we find that measuring the coherence lifetime under a π -pulse echo train with the Carr-Purcell-Meiboom-Gill (CPMG) sequence can be complicated by rf inhomogeneities, which introduce stimulated echoes, whose decay is governed by a mix of longitudinal and transverse relaxation. For this reason, we employ the Phase Incremented Echo Train Acquisition [16] (PIETA) sequence, which eliminates these stimulated echo artifacts and provides a more accurate measure of the spin-echo decays and any J modulations. While PIETA gives a more accurate measurement of the upper limit for the echo train coherence lifetime, inhomogeneities in the rf field strength can still bias the measured lifetime toward lower values.

2. Methods

2.1. Silicate glass preparation

Table 1 gives the compositions of the series of alkali and alkaline earth silicate glass samples prepared for this study. The addition of the alkali or alkaline earth oxides to a silica melt causes depolymerization of the silicate network. This depolymerization leads to the formation of five types of SiO_4 tetrahedra, each characterized by its connectivity, i.e., the number of oxygen that are corner-linked to other tetrahedral [17,18]. These are designated with the notation Q^n , where $n(\sim 0-4)$ represents the number of bridging oxygen per tetrahedron.

Prior to synthesis, the precursors Li₂CO₃ (Aldrich, ACS reagent grade), Na₂CO₃ (Aldrich, 99.99%), CaCO₃ (Aldrich, ACS reagent grade), BaCO₃ (Alfa Aesar, 99.997%), K₂CO₃ (Aldrich, ACS reagent grade) and SiO₂ (Alfa Aesar, 99.99%) were placed in a dehydrating oven under vacuum and at 100 °C overnight to remove water from the materials. Stoichiometric amounts were ground together to ensure homogeneity, and decarbonated overnight. Decarbonization of Li₂CO₃ and CaCO₃ was done at 900 °C, Na₂CO₃ at 700 °C, K₂CO₃ at 950 °C and BaCO₃ at 1300 °C. Batches of approximately 6 g were melted in a 20 cm³ platinum crucible at the temperatures given in Table 1 for 30 min before quenching into a glass by placing the bottom of the crucible in water. This melt procedure was repeated 1 to 3 times, depending on the glass composition, as indicated in Table 1.

All but two glasses were subsequently ground with $\sim 8 \text{ mmol/mol}$ CoO (Alfa Aesar, 99.9995%) followed by another melt and quench procedure to enhance longitudinal relaxation rates. The CoO-doped glass compositions are designated with an asterisk. All doped glasses had a blue tint. In the case of the calcium silicate glass, this CoO doping reduced the spin-lattice relaxation time of ^{29}Si from 2260 s to 37 s. The importance of using Co(II) as the paramagnetic dopant is that it significantly reduces the ^{29}Si T_1 times while causing only minor decreases in T_2 (see Table 4). Despite attempts to clean

Table 1 Sample identification and compositions along with melt procedure used in this study. Compositions marked with an asterisk are doped with 8 mmol/mol of CoO. The number of times the melt procedure was repeated for each glass composition is given in parentheses next to the melt temperature, T_m , in the last column.

Sample ID	Composition	T _m /°C
33Na:67Si 40Ca:60Si 33Li:67Si* 33Na:67Si* 33K:67Si* 40Ca:60Si* 33Ba:67Si*	0.33 Na ₂ O·0.67 SiO ₂ 0.4 CaO·0.6 SiO ₂ 0.327 Li ₂ O·0.665 SiO ₂ ·0.008 CoO 0.327 Na ₂ O·0.665 SiO ₂ ·0.008 CoO 0.327K ₂ O·0.665 SiO ₂ ·0.008 CoO 0.397 CaO·0.595 SiO ₂ ·0.008 CoO 0.327 Ba ₂ O·0.665 SiO ₂ ·0.008 CoO	1100 (×2) 1550 (×3) 1200 (×2) 1100 (×1) 1300 (×2) 1550 (×1) 1500 (×2)

the platinum crucibles in hydrofluoric acid after each synthesis, some paramagnetic contaminants leached out of the crucibles and into the melts during glass synthesis. This contamination may be responsible for some variation in paramagnetic concentrations of the samples.

2.2. NMR measurements

Nuclear magnetic resonance spectroscopy measurements were performed at room temperature on a hybrid Tecmag Apollo-Chemagnetics CMX II 9.4 T NMR spectrometer using a 4 mm Chemagnetics MAS probe. Glass samples were ground and packed in NMR rotors under inert conditions in a nitrogen-filled glove box. Undoped samples were measured on a Bruker Avance III HD 9.4 T NMR spectrometer using a 7 mm Bruker MAS probe. The stability of the spinning speed was ± 2 Hz. The magic angle was set with the 2 H signal of deuterated hexamethylbenzene.

The natural abundance 29 Si static and MAS spectra are shown in Fig. S1 of the Supplemental Material. The line shapes of the highest speed MAS spectra are unresolved as inhomogeneous broadenings dominate due to a distribution of isotropic chemical shifts [19]. With all glasses at or near the disilicate composition, these spectra are dominated by Q^3 sites, which span a range of -94 ppm to -89 ppm. The isotropic line widths for the modified silicate glasses increase with increasing cation potential (i.e., the charge-to-radius ratio, Z/r) of the modifier cations, which cause greater depolymerization of the silicate network [19]. The full width at half maxima of the MAS spectra, given in Table 2, range from around 10 ppm for glasses with lower potential modifiers, such as potassium and sodium, to around 20 ppm for glasses with the higher potential modifiers, such as calcium.

2.2.1. Magnetization recovery

Longitudinal magnetization recoveries were measured using the saturation recovery sequence [20] with logarithmically spaced recovery times. The ²⁹Si T_1 measurements were performed with CPMG echo train acquisition for signal enhancement. Experimental acquisition parameters are summarized in Table S1 of the Supplemental Material. The $\pi/2$ pulse lengths for ²⁹Si varied from 6.5 to 7.6 μ s. All ⁷Li NMR transitions were excited with $\pi/2$ pulse lengths of 7.5 μ s. For ²³Na, only the central $m_I = -\frac{1}{2} \rightarrow \frac{1}{2}$ transition was excited using a selective $\pi/2$ pulse of 10 μ s duration. Magnetization recoveries were fit to the stretched exponential function,

$$M_z(t) = M_z(\infty) \cdot \left[1 - \exp\left[-(t/T_1)^{\beta_1} \right] \right], \tag{2}$$

where T_1 is the longitudinal magnetization recovery time and β_1 is the Kohlrausch exponent. The stretched exponential function is used to account for a distribution of relaxation times. The best-fit parameters are given in Table 2.

Table 2
The NMR line shape modes, $\delta_{\rm iso}^{(\rm mode)}$, full width at half maxima, $\Delta \delta^{\rm MAS}$, and spin-lattice relaxation parameters, T_1 and β_1 , from the MAS spectra of glasses measured in this study. Here, $\chi^2_{\rm v}$ is the reduced chi-square for the fit to Eq. (2) and $\tau_{1.95\%}$ is the 95% recovery time for the longitudinal magnetization. Compositions marked with an asterisk are doped with 8 mmol/mol of CoO.

Sample	Nuclide	$\delta_{ m iso}^{(m mode)}/ m ppm$	$\Delta\delta^{ ext{MAS}}/ ext{ppm}$	T_1/s	eta_1	$ au_{1,95\%}/ ext{s}$	χ^2_v
33Li:67Si*	²⁹ Si	-89	16	38 ± 1	0.64 ± 0.02	210 ± 10	1.38
33Na:67Si	²⁹ Si	-88	10	1900 ± 100	$\boldsymbol{0.79 \pm 0.01}$	7800 ± 500	1.48
33Na:67Si*	²⁹ Si	-87	11	47 ± 1	0.61 ± 0.01	185 ± 8	7.94
33K:67Si*	²⁹ Si	-89	11	81 ± 3	$\boldsymbol{0.59 \pm 0.01}$	510 ± 30	9.47
40Ca:60Si	²⁹ Si	-87	20	2260 ± 60	0.61 ± 0.06	13800 ± 500	4.21
40Ca:60Si*	²⁹ Si	-86	21	37 ± 1	0.65 ± 0.02	203 ± 9	16.3
33Ba:67Si*	²⁹ Si	-91	17	68 ± 4	0.65 ± 0.01	360 ± 20	13.3
33Li:67Si*	⁷ Li	-	5	0.351 ± 0.007	1.00 ± 0.02	1.05 ± 0.03	5.02
33Na:67Si*	²³ Na	-	41	0.0233 ± 0.0003	0.63 ± 0.01	0.131 ± 0.003	7.51

2.2.2. π -Pulse echo train coherence lifetimes

All π -pulse echo-train coherence lifetimes were measured using the Phase Incremented Echo Train Acquisition [16] (PIETA) sequence illustrated in Fig. 1. Additional details on its implementation and signal processing are given in the caption of Fig. 1. For all measurements, a recycle delay, τ_0 , was chosen to ensure 95% recovery of the equilibrium magnetization. A complete list of pulse lengths and other acquisition parameters are given in Tables S2 and S3 of the Supplemental Material.

We use the full width at half maximum (FWHM) of the Fourier transform of the π -echo train decay, Λ , as a measure of the residual ²⁹Si line width after averaging with a π -pulse train and MAS. While some readers might prefer the symbol T_2' as the constant characterizing the coherence lifetime [21], we avoid this usage as it conflicts with the earlier and still common literature usage of T_2' , originally defined by Bloembergen, Purcell and Pound, as the contribution to T_2 from the spectral density function at zero frequency, i.e., the *secular* contribution [22–24]. We prefer the use of FWHM as it is intentionally vague concerning the nature of the broadening mechanism, i.e., coherent or incoherent processes. We determine the FWHM by modeling the echo train decay with a stretched exponential function

$$S(t_1) = A \exp\left[-(\lambda t_1)^{\beta}\right],\tag{3}$$

where λ is the decay rate constant of the transverse magnetization during a train of π pulses [25] and β is the Kohlrausch exponent that accounts for differential relaxation among sites. The FWHM is obtained from an analysis of the numerical Fourier transform of Eq. (3).

Even at a 29 Si natural abundance of 4.67%, there is a nonnegligible number of 29 Si nuclei involved in direct and indirect homonuclear couplings across 29 Si-O- 29 Si linkages. In pure silica glass, for example, 82.6% of the 29 Si resonances do not experience homonuclear couplings, while 16.2% exhibit two spin couplings, and the remaining 1.2% exhibit three and four spin couplings [2]. The fraction of 29 Si nuclei experiencing homonuclear couplings decrease with increasing modifier cation content. In a network of Q³ sites, for instance, only 12.73% are involved in a two spin coupling.

The direct homonuclear dipolar coupling across a 29 Si-O- 29 Si linkage at \sim 3 Å is on the order of \sim 170 Hz. This dipolar coupling will be present in measurements on static samples but is eliminated with MAS, even at moderate spinning rates.

The geminal ${}^2J_{\text{Si-O-Si}}$ coupling across a ${}^{29}\text{Si-O-}{}^{29}\text{Si}$ linkage ranges from 0 to 25 Hz, depending primarily on the Si-O-Si angles of the two tetrahedra in the linkage [5]. This geminal ${}^2J_{\text{Si-O-Si}}$ coupling, which is not removed by MAS, can lead to a modulation of the ${}^{29}\text{Si}$ echo train amplitude. For two spin-1/2 nuclei coupled through

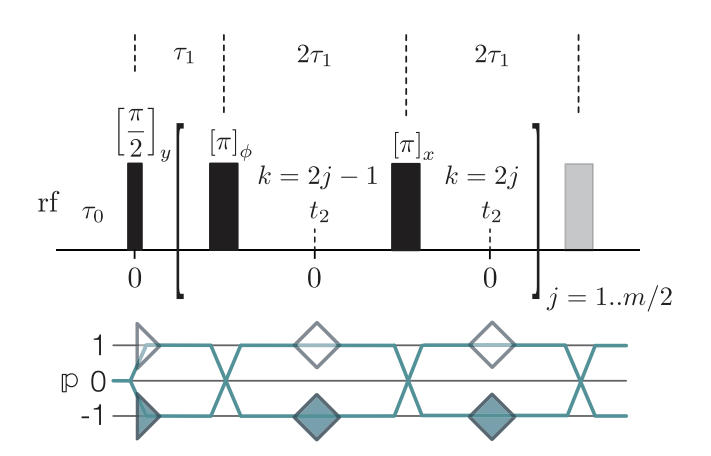


Fig. 1. Graphical representation of the PIETA sequence [16] and \mathbb{P} symmetry pathway [26]. The pulse sequence gives a three dimensional dataset $S(\phi,k,t_2)$, where ϕ is the PIETA phase dimension, k is the echo count dimension, and t_2 is the direct acquisition dimension. To avoid introducing spinning sideband artifacts, the spacing between the centers of adjacent pulses should be an integer multiple of the rotor period. The number of loops for $j=1\dots m/2$ gives a k dimension with m samples. The PIETA phase ϕ is incremented from 0 to 2π along the phase dimension using n_k+2 steps. After a Fourier transform along the phase dimension the echoes with the desired accumulated Δp are selected to reduce the signal to two dimensions: k and t_2 . The k dimension is converted into the echo decay dimension, t_1 , according to $t_1=2k\tau_1$. A Fourier transform of the signal along t_2 followed by a projection of the signal yields a one dimensional dataset decaying along t_1 .

the J interaction, the modulation of the k^{th} echo predominantly follows [27,28]

$$s(k) \propto \cos \left[\pi J k 2 \tau_1 - k \sin^{-1} \left\{ \frac{J \sin(\pi R 2 \tau_1)}{R} \right\} \right],$$
 (4)

where

$$R = \left(\Delta v^2 + J^2\right)^{1/2}.\tag{5}$$

Here Δv is the difference in the chemical shifts of the *J*-coupled spins. From Eq. (4) one finds the well-known behavior that the echo modulation frequency disappears as the strong coupling limit, where $J \gg \Delta v$, is approached,

$$\lim_{R \to I} (k) \to 1. \tag{6}$$

All resonances close to the strong coupling limit exhibit modulation frequencies at or near 0 Hz. From Eq. (4) one can also find in the weak coupling limit, where $J \ll \Delta v$, that

$$s(k) \propto \cos\left[\pi J k 2\tau_1 (1 - \operatorname{sinc}(\pi R 2\tau_1))\right]. \tag{7}$$

It is critical to be aware of two limiting behaviors for echo train acquisition in the weak coupling limit. When $2\tau_1$ is large, or more

specifically, $sinc(\pi R2\tau_1)\ll 1$, this expression simplifies to the expected behavior,

$$\lim_{2\tau \to \infty} s(k) \to \cos(\pi J k 2\tau_1). \tag{8}$$

On the other hand, in the limit that $2\tau_1$ goes to zero, i.e., $sinc(\pi R 2\tau_1) = 1$, the echo modulation frequency disappears,

$$\lim_{2\tau_1 \to 0} s(k) \to 1. \tag{9}$$

Thus, even in the weak coupling limit, the J modulation during echo train acquisition deviates from the expected behavior of Eq. (8), instead giving, according to Eq. (7), a $2\tau_1$ dependent echo modulation frequency (sinc function variation of the J splitting) when the inter-echo period is short relative to the inverse of the shift difference. The influence of this effect diminishes as $1/(\pi\Delta v 2\tau_1)$.

The chemical shift anisotropies (CSA) and dipolar couplings in the solid state also play an important role in the detection of *J*-couplings. In a simple Hahn echo experiment, a coupled two spin system in the solid state and the fast MAS limit [29] behaves identical to that of solution state NMR [30] where

$$|\nu_R| > |d\Delta\nu/2\pi J|, |\Delta\nu_{\rm iso}|. \tag{10}$$

Here v_R is the spinning frequency, $d/2\pi$ is the instantaneous dipoledipole coupling frequency, Δv is the difference in the instantaneous chemical shift frequencies, J is the scalar coupling frequency and $\Delta v_{\rm iso}$ is the difference in the isotropic chemical shift frequencies of the connected nuclei. On the other hand, under moderate MAS speeds [29],

$$|\Delta v_{\rm iso}| \lesssim |\Delta v_{\rm ansio}| < |v_R| < |d\Delta v/2\pi J|,\tag{11}$$

the coupled spins mostly remain within a weak coupling limit because the CSA ensures that the instantaneous chemical shifts of the coupled spins are different for most of the time even when the two spins have identical isotropic chemical shifts. In Eq. (11), $\Delta v_{\rm ansio}$ is the differences in the anisotropic part of the instantaneous chemical shift frequencies.

Because of the disordered network in silicate glasses, there is a distribution of isotropic chemical shifts, CSAs, and direct and indirect dipolar couplings. The isotropic line widths range from 850 Hz in the sodium silicate glass to 1740 Hz in the barium silicate glass. The Q^n anisotropic line shapes have spans ranging from 20 ppm for Q^4 and Q^0 sites to 30–90 ppm for the other Q^n sites [1,19,31,32]. At 9.4 T, this corresponds to an anisotropy that spans \sim 1.5 kHz for Q^4 and Q^0 sites and 2.5 to 7.5 kHz for the other Q^n sites. Thus, with $v_R = 14$ kHz, we find that the majority of the coupled spin systems in silicate glasses would reside within the moderate MAS condition, Eq. (11), and would result in echoes that are modulated by J-coupling as $\cos(\pi Jt)$, i.e., the weak coupling limit.

The J modulations were measured in the natural abundance ²⁹Si PIETA echo train amplitudes for all the glass compositions in this study except the lithium disilicate glass whose ²⁹Si coherence lifetimes were too short to observe any modulation. The J modulation measurements used $2\tau_1$ values of 20 to 40 ms to minimize any sinc function variation of the J splitting.

The modulated echo train amplitudes are modeled using the expression proposed by Srivastava et al. [2],

$$S(t_1) = A \exp\left[-(\lambda t_1)^{\beta}\right] \times \left[(1 - P) + P \exp\left(-\frac{1}{2}\pi^2 t_1^2 \sigma_J^2\right) \cos\left(\pi t_1 \mu_J\right)\right], \tag{12}$$

where P=0.1273 is the fraction of ²⁹Si experiencing a geminal J coupling and μ_J and σ_J are the mean and standard deviation of a Gaussian distribution of the geminal $^2J_{\text{Si}-0-\text{Si}}$ couplings present in the glass. Least-squares fits of the echo top amplitudes to Eq. (12)

are shown as the solid blue line in Fig. 2 with corresponding residuals shown as solid blue lines below each plot. The best-fit parameters are given in Table 3. To highlight the I coupling modulation behavior contained in the small fraction (12.73%) of the total echo amplitude, we plot the values predicted using Eq. (3) with the best-fit amplitude, i.e., A(1-P), decay constant, λ , and Kohlrausch exponent, β , in green dashed lines. More illustrative, however, are the differences between values predicted using Eq. (3) and the experimental echo amplitudes, shown as the green dashed lines below each plot, and where the J modulations are more clearly seen. The mean 29 Si geminal $^{2}J_{Si-0-Si}$ couplings obtained are in good agreement with previously reported results for Q3 species obtained in isotopically enriched samples [15]. The mean μ_I and σ_J values in Table 3 for each glass composition were used as constants in leastsquares fits of other PIETA signals to Eq. (12) as a function of MAS speed, v_R , and π -pulse spacing, $2\tau_1$. These results are summarized in Table 4.

Additionally, we measured the PIETA signal for all glass compositions under static conditions. These echo amplitude decays were fit to Eq. (3) and are summarized in Table 5.

3. Results

We obtain a ²⁹Si MAS-PIETA FWHM of 0.100 Hz in Table 3 using the best-fit parameters to Eq. (12) for silica glass as measured by Srivastava et al. [2]. As noted [2], this particular glass had a blue tint after doping with CoO at levels estimated to be below 100 ppm. Given the few NMR active nuclei in silica glass, this FWHM is attributed to paramagnetic relaxation and serves as a lower limit for comparison to the network-modified silicate glasses.

In Fig. 3A and 3B are selected ²⁹Si PIETA FWHM values of the silicate glasses in this study measured under static and MAS conditions, respectively, and plotted against the mean magnitude of the network modifier cation nuclear magnetic dipole moments, weighted by their natural abundance, that is,

$$\langle |\mu_I| \rangle = \sum p_k |\mu_{I,k}|,\tag{13}$$

where p_k is the natural abundance of the kth isotope for the element.

The ^{29}Si static-PIETA FWHM values in Fig. 3A are all obtained using a $\pi\text{-pulse}$ spacing of $2\tau_1=1$ ms. There is a marked rise in the ^{29}Si static-PIETA FWHM for the higher mean nuclear magnetic dipole moment magnitudes, suggesting that the heteronuclear dipolar coupling is the primary factor in determining the $\pi\text{-pulse}$ echo train decay in those cases. The FWHM of the glasses with lower mean nuclear magnetic dipole moment magnitudes are roughly constant at $\Lambda_{\text{static}}\approx25\,\text{Hz}$. These lower FWHM values are consistent with the coherence lifetimes dominated by homonuclear $^{29}\text{Si-}^{29}\text{Si}$ dipolar couplings, which the $\pi\text{-pulse}$ train cannot refocus.

To obtain the range of homonuclear dipolar couplings between ²⁹Si nuclei, we take the probability distribution of ²⁹Si distances as given by

$$p(r) = \frac{3}{r_s} \left(\frac{r}{r_s}\right)^2 e^{-(r/r_s)^3},$$

where r_s is the Wigner-Seitz radius, defined by

$$\frac{4}{3}\pi r_s^3 = \frac{1}{\rho_n},$$

and ρ_n is the number density of ²⁹Si nuclei per unit volume in the sample, given by

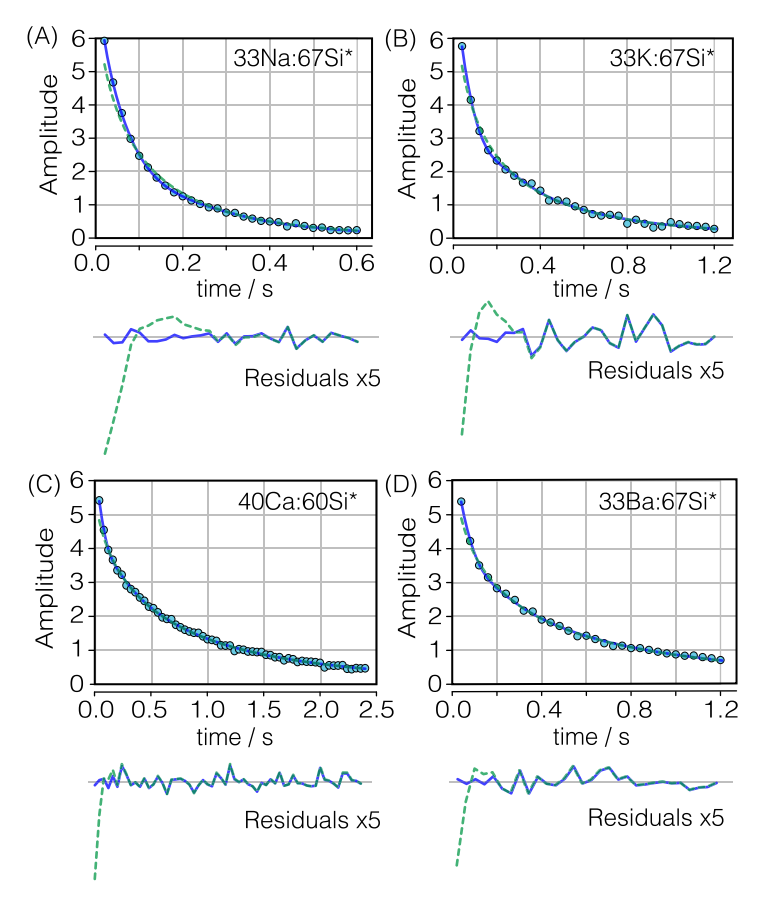


Fig. 2. Plots of the ²⁹Si MAS-PIETA echo top amplitudes as a function of echo time for glass compositions (A) 33Na:67Si*, (B) 33 K:67Si*, (C) 40Ca:67Si* and (D) 33Ba:60Si*. Solid blue lines are the best-fit curve obtained from a least-squares analysis of the experimental data with Eq. (12). The corresponding residuals are shown as solid blue lines below each plot. The dashed green lines represent the predicted curve from Eq. (3), i.e., without *J* modulation, using the amplitude, A(1 - P), decay constant, λ , and Kohlrausch exponent, β , obtained from the best fit to Eq. (12) in Table 3. The dashed green lines below each plot show the difference between the experimental amplitudes and those predicted from Eq. (12).

Table 3Best fit parameters from a least-squares analysis of ²⁹Si MAS-PIETA echo amplitudes of alkali and alkaline-earth silicate glasses using Eq. (12) in a system with P = 12.73% of the spins involved in a weak geminal J coupling. Here ν_R is the spinning frequency, $2\tau_1$ is the spacing between π pulses, μ_J and σ_J are the mean and standard deviation of the J coupling distribution, λ^{-1} is the inverse echo train decay time constant, β is the Kohlrausch exponent, and χ_{ν}^2 is the reduced chi-square. The FWHM, Λ , is obtained from a numerical Fourier transform of Eq. (3) using the best-fit parameters λ and β . Compositions marked with an asterisk are doped with 8 mmol/mol of CoO.

Sample	v_R/kHz	$2\tau_1/ms$	$\mu_{\!J}$ /Hz	$\sigma_J/{ m Hz}$	λ^{-1}/ms	β	χ^2_{ν}	Λ/Hz
SiO ₂ * from Ref. [2]	14.286	40	12.51 ± 0.06	4.55 ± 0.06	967 ± 4	0.55 ± 0.001	2.5	0.100 ± 0.001
33K:67Si*	14	40	5.3 ± 0.4	2.0 ± 0.4	136 ± 10	0.56 ± 0.03	1.50	$\boldsymbol{0.75 \pm 0.06}$
33Na:67Si*	14	20	5.2 ± 0.3	2.0 ± 0.3	84 ± 4	0.65 ± 0.02	0.37	1.8 ± 0.1
33Ba:67Si*	14	40	5.1 ± 0.6	3.9 ± 0.6	223 ± 20	0.51 ± 0.02	1.22	0.34 ± 0.03
40Ca:60Si*	14	40	4.2 ± 0.5	3.6 ± 0.5	527 ± 20	0.62 ± 0.01	0.75	0.26 ± 0.01

$$\rho_n(^{29}\mathrm{Si}) = \frac{f(^{29}\mathrm{Si})\,n_\mathrm{Si}}{n_\mathrm{Glass}}\,\frac{N_A\rho}{M}. \tag{14}$$

Here, $f(^{29}\text{Si})$ is the ^{29}Si abundance, N_A is the avogadro constant, M is the molar mass for a given chemical composition, n_{Si} is the stoichiometry of silicon in the chemical composition, n_{Glass} is the stoichiometry of the glass in the chemical composition, and ρ is the mass density. This distance distribution peaks at $r_{\text{mode}} \approx 0.874r_s$. Using the glass densities, given in Table S4, the predicted ^{29}Si homonuclear dipolar couplings give static-PIETA FWHM values that are consistent with the values observed in Fig. 3A for the potassium, barium, and calcium silicate glasses.

With moderate MAS speeds these ²⁹Si homonuclear dipolar couplings are removed, and a more linear correlation between ²⁹Si MAS-PIETA FWHM and mean nuclear magnetic dipole moment magnitudes is obtained. This is illustrated in Fig. 3B, where the

smallest ²⁹Si MAS-PIETA FWHM values from each (Co-doped) glass composition in Table 4 are plotted as a function of mean nuclear magnetic dipole moment magnitudes. ¹ Under MAS conditions, the ²⁹Si echo train coherence lifetimes are limited by the heteronuclear dipolar couplings to the abundant NMR active nuclei of the alkali cations

The ²⁹Si MAS-PIETA FWHM in the alkaline earth silicate glasses are closest to the value obtained for pure silica glass. This similarity is because the NMR active isotopes of the alkaline earth cations are lower in abundance and have lower magnitude magnetic dipole moments than the alkali cations. For example, the only NMR active calcium isotope, ⁴³Ca, has a natural abundance of 0.135% and a

 $^{^{\}rm 1}$ These values correspond to 4.1 Hz for Li, 1.8 Hz for Na, 0.75 Hz for K, 0.25 Hz for Ca, and 0.32 Hz for Ba.

Table 4

Best fit parameters of 29 Si MAS-PIETA echo amplitudes under MAS obtained using Eq. (12) with P=12.73%, for selected alkali and alkaline earth silicate glasses, except the 33Li:67Si* composition which was obtained using Eq. (3). Here ν_R is the spinning frequency, $2\tau_1$ is the spacing between π pulses, $n_{\rm echo}$ represents the number of echoes collected, n_{ϕ} is the number of phases used in the PIETA measurement, λ^{-1} is the echo train decay time constant, β is the stretch exponent, and χ^2_{ν} is the reduced chi-square of the fit. In the fits to Eq. (12), the values for μ_J and σ_J were locked to the corresponding values in Table 3. Values of pure silica glass were taken from Ref. [2] for comparison (with P=14.4%). The FWHM is obtained from a numerical Fourier transform of Eq. (3) using the best-fit parameters λ and β . Compositions marked with an asterisk are doped with 8 mmol/mol of CoO.

Sample	v_R/kHz	$2\tau_1/ms$	λ^{-1} /ms	β	χ^2_{ν}	Λ/Hz
33Li:67Si*	3.5	8	8 ± 2	0.60 ± 0.06	1.16	16 ± 4
33Li:67Si*	7	8	20 ± 2	0.62 ± 0.03	0.87	6.8 ± 0.7
33Li:67Si*	14	8	38 ± 2	0.66 ± 0.02	2.33	4.1 ± 0.2
33Na:67Si*	3.5	16	28 ± 6	0.54 ± 0.04	1.26	3.3 ± 0.7
33Na:67Si	7	40	54 ± 5	0.60 ± 0.02	1.47	2.3 ± 0.2
33Na:67Si*	7	20	58 ± 4	0.60 ± 0.02	0.51	2.1 ± 0.2
33Na:67Si*	7	16	63 ± 3	0.64 ± 0.02	0.64	2.3 ± 0.1
33Na:67Si*	14	60	77 ± 10	0.69 ± 0.05	1.35	2.3 ± 0.3
33Na:67Si*	14	40	70 ± 8	0.63 ± 0.03	1.38	2.0 ± 0.2
33Na:67Si*	14	20	84 ± 3	0.65 ± 0.01	0.35	1.8 ± 0.06
33Na:67Si*	14	16	89 ± 4	0.67 ± 0.02	0.45	1.8 ± 0.1
33Na:67Si*	14	10	80 ± 4	0.63 ± 0.02	1.53	1.8 ± 0.1
33Na:67Si*	14	4	57 ± 2	0.58 ± 0.02	0.67	2.0 ± 0.1
33Na:67Si*	14	2	43 ± 2	0.57 ± 0.02	0.60	2.5 ± 0.1
33K:67Si*	3.5	40	68 ± 20	0.58 ± 0.06	0.92	1.7 ± 0.5
33K:67Si*	7	40	90 ± 10	0.59 ± 0.03	0.87	1.3 ± 0.2
33K:67Si*	14	40	135 ± 10	0.56 ± 0.02	0.84	0.75 ± 0.06
40Ca:60Si*	3.5	40	496 ± 30	0.61 ± 0.03	0.83	0.26 ± 0.02
40Ca:60Si	7	800	650 ± 200	0.52 ± 0.05	1.05	0.13 ± 0.06
40Ca:60Si*	7	40	513 ± 20	0.63 ± 0.02	0.91	0.28 ± 0.01
40Ca:60Si*	14	160	495 ± 40	0.60 ± 0.02	1.09	0.25 ± 0.02
40Ca:60Si*	14	40	527 ± 10	0.62 ± 0.01	0.85	0.257 ± 0.005
40Ca:60Si*	14	20	417 ± 10	0.63 ± 0.01	1.68	$\boldsymbol{0.338 \pm 0.008}$
40Ca:60Si*	14	10	278 ± 9	0.57 ± 0.02	0.59	0.39 ± 0.01
40Ca:60Si*	14	4	143 ± 2	0.57 ± 0.01	0.33	0.75 ± 0.01
33Ba:67Si*	3.5	40	195 ± 20	0.49 ± 0.03	0.82	0.33 ± 0.04
33Ba:67Si*	7	120	230 ± 40	0.50 ± 0.03	1.43	0.31 ± 0.04
33Ba:67Si*	7	40	220 ± 20	0.50 ± 0.03	1.02	0.32 ± 0.03
33Ba:67Si*	7	20	212 ± 7	0.56 ± 0.01	1.12	0.48 ± 0.02
33Ba:67Si*	14	40	237 ± 20	0.52 ± 0.02	1.35	0.34 ± 0.03

Table 5Best fit parameters from a least-squares analysis of ²⁹Si PIETA echo amplitudes in static samples of alkali and alkaline earth silicate glasses obtained using Eq. (3). Here, $2\tau_1$ is the spacing between π pulses, n_{echo} represents the number of echoes collected, n_{ϕ} is the number of phases used in the PIETA measurement, λ^{-1} is the echo train decay time constant, β is the stretch exponent, and χ^2_{τ} is the reduced chi-square of the fit. The FWHM is obtained from an analysis of the numerical Fourier transform of Eq. (3) using the best-fit parameters. Compositions marked with an asterisk are doped with 8 mmol/mol of CoO.

Sample	$2\tau_1/ms$	λ^{-1} /ms	β	χ^2_{ν}	Λ/Hz
33Li:67Si*	2	0.3 ± 0.7	0.49 ± 0.2	0.82	220 ± 200
33Li:67Si*	1.4	0.4 ± 0.1	0.48 ± 0.04	0.94	153 ± 40
33Li:67Si*	1	1.3 ± 0.2	0.63 ± 0.05	0.98	108 ± 20
33Li:67Si*	0.6	2.1 ± 0.2	0.67 ± 0.03	1.02	78 ± 7
33Li:67Si*	0.2	3.4 ± 0.1	$\boldsymbol{0.74 \pm 0.02}$	0.71	59 ± 2
33Na:67Si*	2	1 ± 0.4	0.52 ± 0.06	0.93	81 ± 40
33Na:67Si*	1	3.3 ± 0.4	0.67 ± 0.05	0.54	49 ± 6
33Na:67Si*	0.6	4.2 ± 0.4	0.73 ± 0.05	0.63	46 ± 4
33Na:67Si*	0.2	4.2 ± 0.2	$\boldsymbol{0.74 \pm 0.04}$	0.24	48 ± 2
33K:67Si*	1	6.5 ± 0.4	$\boldsymbol{0.70 \pm 0.03}$	0.90	28 ± 2
40Ca:60Si	6	13 ± 1	0.91 ± 0.05	1.55	22 ± 2
40Ca:60Si*	4	12.9 ± 0.8	0.88 ± 0.04	1.44	21 ± 1
40Ca:60Si*	2	12.3 ± 0.5	0.89 ± 0.03	2.07	22 ± 1
40Ca:60Si*	1	9.0 ± 0.3	0.84 ± 0.03	1.88	28 ± 1
40Ca:60Si*	0.6	7.7 ± 0.2	0.81 ± 0.03	0.76	31 ± 1
40Ca:60Si*	0.2	4.1 ± 0.1	0.76 ± 0.03	0.40	51 ± 1
33Ba:67Si*	1	9.6 ± 0.3	0.81 ± 0.02	2.12	24.5 ± 0.8

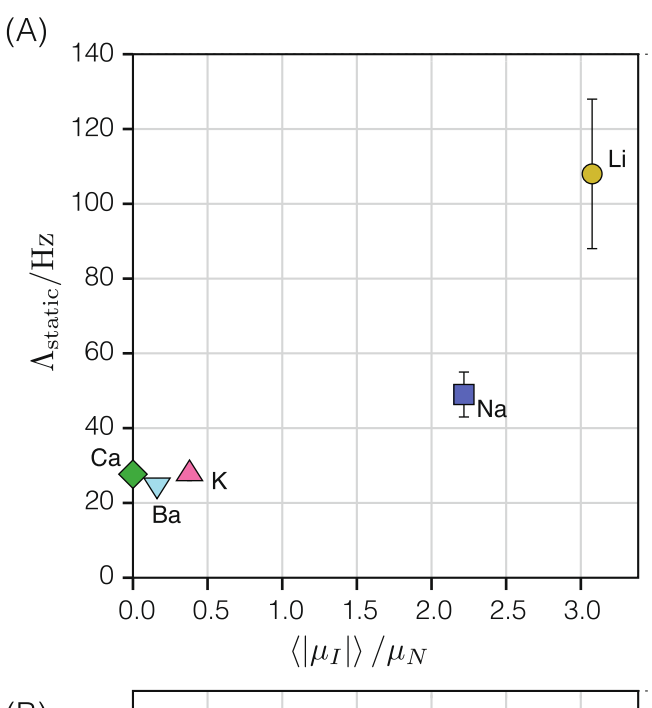
magnetic dipole moment that is 2.5 times smaller in magnitude than ${}^{7}\text{Li}$.

Fig. 4 is a plot of the ²⁹Si MAS-PIETA FWHM for the (Co-doped) glasses as a function of rotor period. For the lithium, sodium, and potassium silicate glasses, we observe an approximately linear relationship between the rotor period and the ²⁹Si FWHM. In con-

trast, the 29 Si MAS-PIETA FWHM values in the alkaline earth silicate glasses (barium and calcium) are invariant to rotor period, i.e., beyond a much lower spinning frequency threshold required to eliminate the homonuclear 29 Si- 29 Si dipolar couplings. We can approximate the trend in FWHM with rotor period at a constant π -pulse spacing as given by

Table 6Best fit parameters from a least-squares analysis of the ²⁹Si MAS-PIETA FWHM values in Fig. 4 using Eq. (15).

Sample	$2\tau_1/ms$	$b_R/(Hz/s)$	$\Lambda_{R,0}/{ m Hz}$
33Li:67Si*	8	$41,800 \pm 7500$	1.1 ± 0.6
33Na:67Si*	16	7000 ± 1500	1.3 ± 0.2
33K:67Si*	40	5700 ± 1600	0.35 ± 0.14



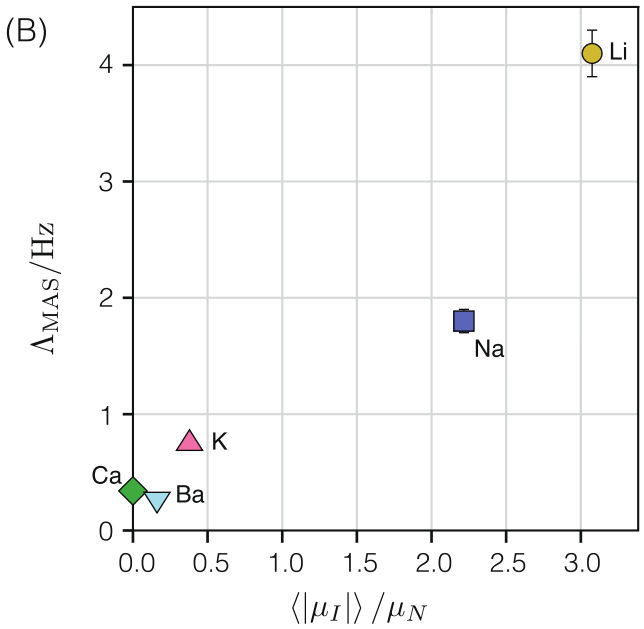


Fig. 3. The ²⁹Si PIETA FWHM values of alkali and alkaline-earth silicate glasses in this study under (A) static and (B) MAS ($\nu_R=14\text{kHz}$) conditions versus the mean magnitude of the network modifier nuclear magnetic dipole moments in units of nuclear magnetons. The π -pulse spacing in static sample measurements shown above is $2\tau_1=1$ ms. For the spinning samples, the π -pulse spacing is $2\tau_1=8$ ms for 33Li:67Si*, $2\tau_1=16$ ms for 33Na:67Si*; and $2\tau_1=40$ ms for 33 K:67Si*, 33Ba:67Si* and 40Ca:60Si*.

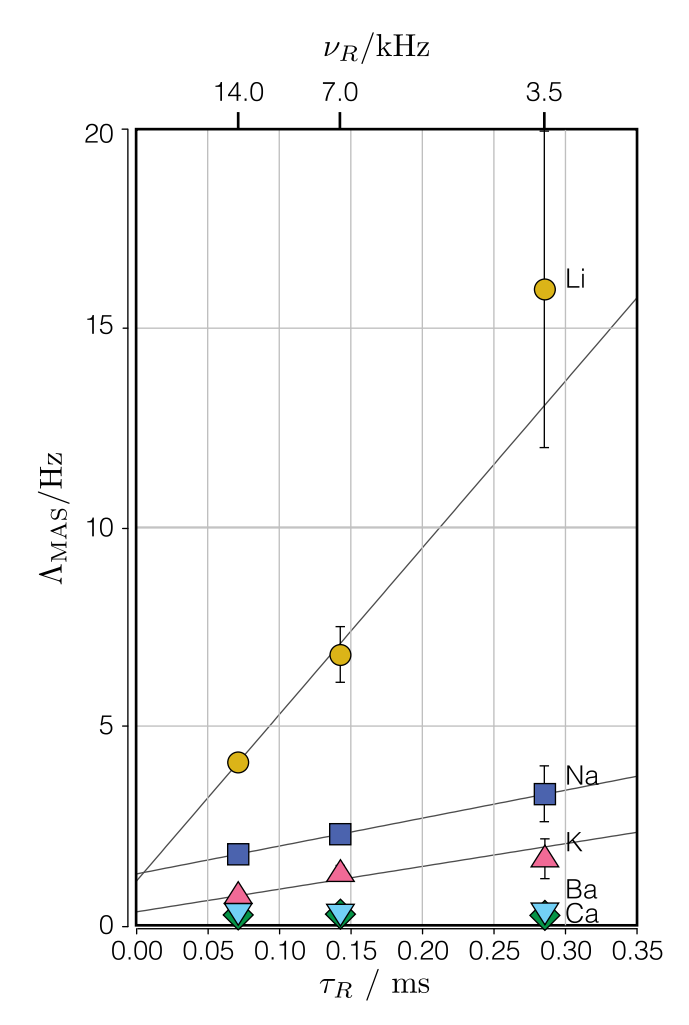


Fig. 4. The ²⁹Si MAS-PIETA FWHM values for alkali and alkaline earth silicate glasses in this study as a function of the rotor period τ_R . The 2 τ_1 periods used for π -pulse echo train acquisition for each composition are 8 ms for 33Li:67Si* (circles), 16 ms for 33Na:67Si* (squares); and 40 ms for 33K:67Si* (triangles), 33Ba:67Si* (inverted triangles) and 40Ca:60Si* (diamonds). Solid lines where obtained from least-squares fits of FWHM values to Eq. (15).

$$\Lambda_{\text{MAS}}(\tau_R) = b_R \tau_R + \Lambda_{R,0}. \tag{15}$$

The solid lines in the plot are the best fits. The differences in the intercept $\Lambda_{R,0}$ likely arise from variations in paramagnetic doping levels. As expected, glasses with modifier cations having larger mean magnetic moments require faster spinning speeds to extend 29 Si echo train lifetimes.

In the magnetically dilute alkaline earth silicates, as well as in silica glass, the paramagnetic dopant plays the dominant role in determining the ²⁹Si MAS-PIETA FWHM. For comparison, a calcium silicate glass composition was prepared without Co doping. Its ²⁹Si MAS-PIETA FWHM is 0.13 Hz, approximately half the width of the same glass composition with Co doping, and nearly identical to the ²⁹Si MAS-PIETA FWHM of silica glass.

In Fig. 5A and 5B are selected 29 Si PIETA FWHM values of the silicate glasses in this study measured under static and MAS conditions, respectively, as a function of the π -pulse spacing. Due to the rf inhomogeneities, it is impossible to have a refocusing pulse that is perfect for all spins. Therefore, with every π pulse, a portion of the magnetization will not be refocused, leading to a broadening of the Fourier transform of the echo train. This effect becomes more significant with increasing pulse rates and is more evident for longer-lived magnetizations, as is visible in Figs. 5 when com-

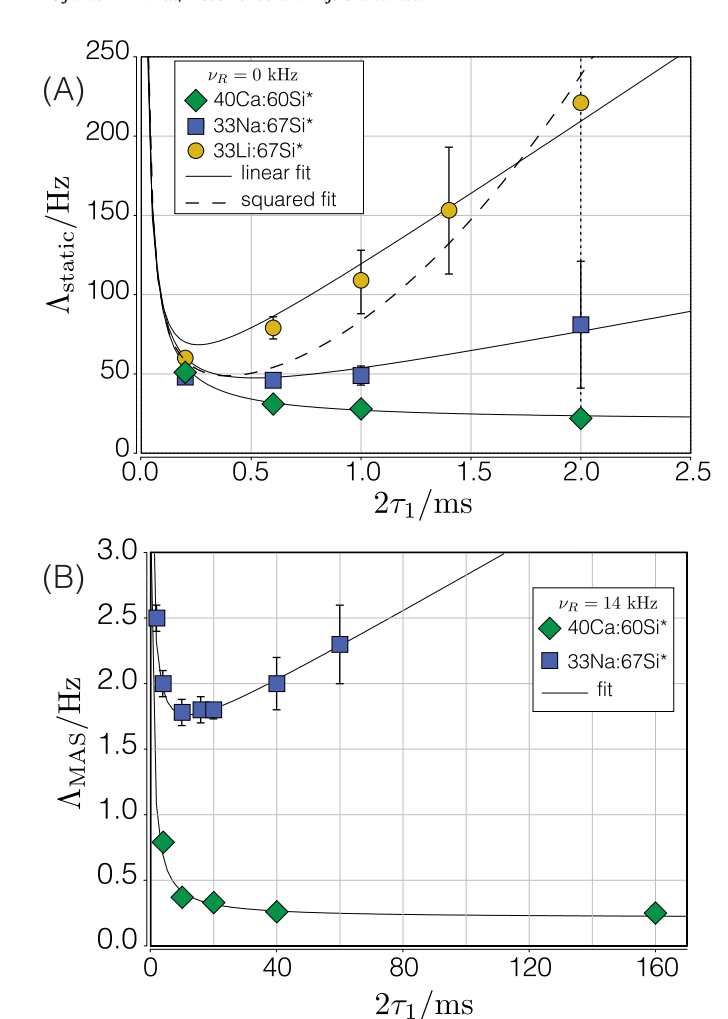


Fig. 5. The ²⁹Si PIETA FWHM values of silicate glasses in this study under (A) static and (B) MAS ($\nu_R=14$ kHz) conditions as a function of the π -pulse spacing $2\tau_1$. Glass compositions are 33Li:67Si* (circles), 33Na:67Si* (squares) and 40Ca:60Si* (diamonds). The solid lines represent the best fit curves from a least-squares fit of the ²⁹Si PIETA FWHM to Eq. (17). The dashed line represents the curve from the best fit of the 33Li:67Si* ²⁹Si PIETA FWHM to Eq. (22).

paring the FWHM of sodium and lithium silicate glasses to those of the calcium silicate glass. The loss of coherence due to π pulse angle missetting and rf inhomogeneities can be approximated as an additional exponential decay, leading to an inverse dependence of the FWHM on the π -pulse spacing, given by

$$\Lambda^*(2\tau_1) = \frac{c_\pi}{2\tau_1}.\tag{16}$$

This contribution becomes the dominant broadening mechanism in the limit of short $2\tau_1$ values. Note that the c_π coefficient is a function of the rf homogeneity of the probe rather than the sample. Thus, we approximate the FWHM at a constant MAS speed as a sum of contributions, neglecting the line shape effects of any Kohlrausch exponent variation, as given by

$$\Lambda_{\pi}(2\tau_{1}) = b_{\pi}2\tau_{1} + \frac{c_{\pi}}{2\tau_{1}} + \Lambda_{\pi,0}, \tag{17}$$

In the static measurements, $\Lambda_{\pi,0}$ is determined by the dephasing due to the homonuclear ²⁹Si dipolar couplings, as previously mentioned. In the case of MAS, we attribute $\Lambda_{\pi,0}$ to paramagnetic relaxation enhancement, in analogy to $\Lambda_{R,0}$, and note the good agreement of these two values obtained for the sodium silicate glass. Best-fit

parameters for Eq. (17) are given in Table 7. Fig. 5 shows the obtained fits as solid lines through the measured data.

4. Discussion

Based on the results of the previous section, we conclude that paramagnetic relaxation dominates the ²⁹Si MAS-PIETA FWHM in the magnetically dilute alkaline earth silicate glasses. On the other hand, the heteronuclear dipolar couplings to the abundant NMR active nuclides in the alkali cations dominate the ²⁹Si MAS-PIETA FWHM in the alkali silicate glasses. Since MAS-PIETA is capable of removing both incoherent and coherent mechanisms involving the heteronuclear dipolar couplings, we begin by investigating whether the fluctuating heteronuclear dipolar couplings to the NMR active nuclides in the alkali cations can be responsible for these larger ²⁹Si FWHM values.

4.1. ²⁹Si T₂ dipolar relaxation models and regimes

Fluctuations in the heteronuclear dipolar coupling between 29 Si and the NMR active nuclei of the modifier cations can arise through (1) time-dependent variations in the internuclear distance vector between the 29 Si and the modifier cation nuclei, and (2) time-dependent variations in the nuclear spin state of the modifier cation. The former is the result of modifier cation mobility. The latter can result from a combination of modifier cation mobility and spin-lattice relaxation time of the modifier cation nucleus; e.g., if different sodium cations hop in and out of a site near a given 29 Si, part of the heteronuclear dipolar coupling fluctuations result from the random nuclear spin states, i.e., $m_I = -3/2, -1/2, 1/2,$ and 3/2, of the different sodium cations occupying into the site. In the absence of significant modifier cation mobility, the nuclear spin states of a fixed modifier cation will change due to the nuclear spin-lattice relaxation of the modifier cation.

The inverse of the heteronuclear dipolar coupling constant, δ^{-1} , given by

$$\delta^{-1} = \left[\sqrt{\frac{4}{15}} \left(\frac{\mu_0}{4\pi} \frac{\hbar \gamma_1 \gamma_S}{r^3} \right) \sqrt{S(S+1)} \right]^{-1}, \tag{18}$$

gives us an approximate limit for determining whether the correlation time for the dipolar fluctuations falls in the motional narrowing regime ($\tau_c \ll \delta^{-1}$) or in the slow motion regime ($\tau_c \gg \delta^{-1}$). In Table 8 are the nearest-neighbor heteronuclear dipolar coupling distances between silicon and modifier cations approximated using Shannon-Prewitt radii [33] along with corresponding δ and δ^{-1} values. Also given in Table 8 are the nearest-neighbor homonuclear coupling between the given alkali cation nuclei using distances estimated from analogous crystalline compounds.

4.1.1. Random fluctuations of internuclear distances

To obtain the expected correlation times due to modifier cation diffusion in the glass, we use a simple random walk and diffusion model where the jump rate for alkali ions is given by

$$\frac{1}{\tau_c} = 6D/\Gamma^2. \tag{19}$$

Here D is the self-diffusion coefficient and Γ is the jump length. The jump length can be set to $\Gamma = r_{\rm M-M}$ using values taken from Table 8. For example, sodium diffusion coefficients on the order of 10^{-15} to 10^{-16} cm²/s are obtained in sodium silicate glasses using values for D^* from tracer diffusion measurements [34,35], measured at 300 °C and higher, and extrapolated to room temperature using measured activation energies. Alternatively, one can use electrical conductiv-

Table 7Best fit parameters from a least-squares analysis of the ²⁹Si MAS-PIETA FWHM values in Fig. 5 using Eq. (17). Values marked with † were taken from the fits of 40Ca:60Si* and held constant.

Sample	v_R/kHz	$b_{\pi}/(\mathrm{Hz/s})$	$c_{\pi}/(\mathrm{Hz/s})$	$\Lambda_{\pi,0}/Hz$
33Li:67Si*	0	90 ± 4	6.2^{\dagger}	20^{\dagger}
33Na:67Si*	0	24 ± 4	6.2^{\dagger}	20^{\dagger}
40Ca:60Si*	0	-	6.2 ± 0.4	20 ± 1
33Na:67Si*	14	0.014 ± 0.001	2.1^{\dagger}	1.42 ± 0.01
40Ca:60Si*	14	-	2.1 ± 0.1	0.21 ± 0.01

Table 8Nearest neighbor dipolar coupling parameters among relevant nuclei in the alkali and alkaline-earth silicate glasses in this study. Heteronuclear coupling distances are estimated from Shannon-Prewitt radii [33], while homonuclear coupling distances are estimated from analogous crystalline compounds.

			²⁹ Si-M dipolar coupling			M–M dipolar coupling	3
Nucleus	I	r_{Si-M} /Å	$(\delta/2\pi)/Hz$	δ^{-1}/ms	$r_{ m M-M}/ m \AA$	$v_d/{\rm Hz}$	v_d^{-1}/ms
⁷ Li	3/2	3.55	207.5	4.82	2.6	1032	0.969
²³ Na	3/2	3.95	102.6	9.75	3.1	282	3.54
³⁹ K	3/2	4.38	13.3	75.31	3.6	5.6	178.0

ities, σ , which relate to the ionic diffusion coefficient according to the Nernst-Einstein equation,

$$D_{\sigma} = f \frac{\sigma k_B T}{Nq^2}, \tag{20}$$

where k_B is the Boltzmann constant, T the temperature, N the number of charge carriers per volume unit, q the particle charge in Coulomb and f a correction factor, which was set to 0.3 in this analysis [34,35].

Substituting the range of sodium diffusion coefficients in Table 9 and a $\Gamma = 3.1 \,\text{Å}$ hop distance into Eq. (19) gives hopping correlation times in the range of 0.016 s - 1.6 s. This range of values is greater than the value of $\delta^{-1} = 9.75$ ms in Table 8 for the ²⁹Si-²³Na heteronuclear dipolar coupling. Thus, the correlation time of heteronuclear dipolar coupling fluctuations from sodium diffusive motion at room temperature are well within the slow motion regime. Similar calculations performed for other alkali cations in these silicate glasses lead to the correlation times given in Table 9. Again, on the basis of modifier cation diffusive motion at room temperature, the heteronuclear dipolar coupling fluctuations are well within the slow motion regime. Analysis of ⁷Li longitudinal relaxation data by Göbel et al. [36] found a distribution of correlation times in lithium disilicate glasses, with a maximum at around 40 ms at room temperature, consistent with the range of correlation times obtained from the diffusion coefficients in

In the slow motion regime, Vega's expression [14] in Eq. (1), is used to obtain the FWHM, given by

$$\Lambda \sim \frac{\delta^2 \tau_p^2}{2\pi \tau_c}.\tag{21}$$

Substituting the correlation times in Table 9 into Eq. (21) gives the estimates for the 29 Si FWHM given in the last column of Table 9. The predicted 29 Si FWHM due to fluctuating 29 Si– 23 Na heteronuclear dipolar couplings under MAS at a speed of 14 kHz, based on the range of τ_c values in Table 9, are significantly smaller than the observed range of 1.8 Hz – 3.3 Hz in Table 4. Similarly, FWHM predictions due to 29 Si– 7 Li heteronuclear dipolar coupling fluctuations are orders of magnitude smaller than the observed range of 4.1 Hz – 16 Hz in Table 4.

It should be noted that diffusion in a restricted region due to isolated ions or ion clusters can result in no net translational diffusion but still be a source of fluctuating heteronuclear dipolar cou-

plings. However, the concentration of these isolated ions or ion clusters is small in a disilicate glass composition, as most ions participate in percolating channels [37–39].

4.1.2. Random fluctuations of nuclear spin states

Spin lattice relaxation of the NMR active modifier cation nuclei, causing fluctuations of modifier cation nuclear spin states, can also be a possible source of $^{29}\mathrm{Si}$ heteronuclear dipolar fluctuations. Measured $^{23}\mathrm{Na}$ and $^{7}\mathrm{Li}$ T_{1} relaxation times in the corresponding network modified silicate glasses are given in Table 2. These are in good agreement with results reported in the literature [40,36]. The $^{23}\mathrm{Na}$ relaxation times are one order of magnitude shorter than those for $^{7}\mathrm{Li}$ and is likely due to the larger magnitude of the $^{23}\mathrm{Na}$ nuclear electric quadrupole moment. It is also consistent with previous findings that the $^{7}\mathrm{Li}$ and $^{23}\mathrm{Na}$ spin-lattice relaxation arise primarily from fluctuating local electric field gradients at room temperature [41]. While the spin-lattice relaxation times of $^{39}\mathrm{K}$ were not measured, the magnitude of its nuclear quadrupole moments is similar to $^{7}\mathrm{Li}$. Thus, we expect the $^{39}\mathrm{K}$ spin-lattice relaxation times to also be on the order of 1 s.

Taking these nuclear spin-lattice relaxation times of the alkali cation nuclei as the correlation times, τ_c , for the fluctuations in the heteronuclear dipolar couplings with ²⁹Si places this relaxation mechanism in the slow-motion regime. Substituting these τ_c values into Eq. (21) gives ²⁹Si MAS-PIETA FWHM values (not shown) that are orders of magnitude smaller than the values observed for the alkali silicate glasses in Table 4.

Thus, we conclude that fluctuating heteronuclear dipolar couplings arising from either diffusion or alkali nuclear spin relaxation are not responsible for the ²⁹Si FWHM values in the alkali silicate glasses.

4.2. Residual dipolar broadenings

After eliminating all possible mechanisms arising from incoherent processes, we turn our attention to coherent processes, focusing on the heteronuclear dipolar coupling between $^{29}\mathrm{Si}$ and the alkali cation nuclei, as causing the decay of the $^{29}\mathrm{Si}$ π -pulse echo train. While a heteronuclear dipolar coupling of a $^{29}\mathrm{Si}$ to an isolated alkali cation nucleus will be completely averaged away by MAS or a π -pulse train, this will not be the case when a $^{29}\mathrm{Si}$ is coupled to alkali cation nuclei with strong homonuclear couplings among themselves.

Table 9
Correlation time, τ_c , estimates for the modifier cations interstitial jumps based on ionic diffusion coefficients D of disilicate glasses. Here, D^* refers to diffusion coefficients obtained from tracer diffusion measurements, and D_σ is calculated from electrical conductivity measurements. Diffusion data is taken from *Handbook of Glass Properties* [34] by Doremus. The Λ_{MAS} values are estimated using Eq. (21) at a spinning speed of 14 KHz.

M	$D^*/(cm^2/s)$	$D_{\sigma}/(\mathrm{cm}^2/\mathrm{s})$	Γ/Å	$ au_c$	Λ_{MAS}
Li ⁺	10^{-15}	$10^{-14} - 10^{-15}$	2.6	11 ms-113 ms	0.31 mHz-3.2 mHz
Na ⁺	$10^{-15} - 10^{-16}$	$10^{-14} - 10^{-15}$	3.1	16 ms-1.6 s	5.3 μHz-530 μHz
K ⁺	10^{-15}	10^{-15}	3.6	216 ms	0.66 nHz

Maricq and Waugh [12] recognized that a three spin system, S- I_1 - I_2 , has a rotating-frame Hamiltonian that does not commute with itself at all times under MAS or a π -pulse train; and showed that this homogeneous interaction will not fully average away at finite MAS or π -pulse rates. Using Average Hamiltonian Theory (AHT), Maricq and Waugh further showed that the FWHM of the S spin under MAS will decrease linearly with decreasing MAS period. This is consistent with our observations of the 29 Si MAS-PIETA FWHM values as a function of rotor period in Fig. 4.

In the case of static samples, our observation is that the 29 Si PIETA FWHM values decrease linearly with decreasing π -pulse spacing as indicated by the best-fit solid lines in Fig. 5A for the 33Li:67Si* composition at longer $2\tau_1$ spacings. This result, however, is inconsistent with a simple AHT explanation which ignores finite pulse effects and predicts that both the zeroth- and first-order AHT contributions vanish in any symmetric sequence, i.e., $\hat{H}(0+t) = \hat{H}(\tau_p - t)$ [42,43], which is the case for a π -pulse train leading up to the acquisition of even echoes. In this situation, the leading (second-order) contribution in the AHT expansion predicts that the FWHM is proportional to $(2\tau)^2$. However, a best fit of the 29 Si PIETA FWHM values of the 33Li:67Si* composition in Fig. 5A to a $(2\tau)^2$ dependence, i.e.,

$$\Lambda_{\pi}(2\tau_{1}) = b_{\pi}(2\tau_{1})^{2} + \frac{c_{\pi}}{2\tau_{1}} + \Lambda_{\pi,0}, \tag{22} \label{eq:22}$$

shown as a dashed line, gives worse agreement than the 2τ dependence. We speculate that finite π pulse widths (\sim 15 μ s) and rf inhomogeneities spoil the averaging symmetry of the π -pulse train and lead to a reintroduction of the zeroth-and first-order AHT contributions [44]. Additionally, the shifting phase between adjacent π pulses in the PIETA sequence, instead of the unchanging π pulse phases in CPMG, may further lead to this loss of averaging symmetry. In either case, we would expect that these effects should diminish with shorter π pulse lengths at higher rf field strengths.

In the case of MAS, our observation is that the ²⁹Si MAS-PIETA FWHM values decrease linearly with decreasing π -pulse spacing as observed in the best-fit solid line for the 33Na:67Si* composition in Fig. 5B at longer $2\tau_1$ spacings. The combined effect of MAS and a π -pulse train can be analyzed using a second averaging approach [43]. In this approach, the first average is calculated over the shorter rotor period, and the second average is calculated over the longer π -pulse period. While this approach predicts that residual heteronuclear dipolar coupling goes to zero in the simple case of the $S - I_1 - I_2$ system, this will not be true when the heteronuclear dipolar coupling is to a bath of homonuclear coupled nuclei [45,46]. Unfortunately, a second average calculation in the latter case is particularly challenging. Prior to Maricq and Waugh, Kessemeier and Norberg [47] found a linear dependence of the transverse magnetization decay with the spinning speed in a spin system of ³¹P nuclei coupled to a bath of ²⁷Al. A linear dependence on MAS speeds has also been observed in proton linewidths [48,49], and has also been found to affect the coherence lifetime of ²⁹Si through a train of π pulses during MAS [50,51]. Similarly, Hahn echoes and, more practically, a π -pulse train are also known to refocus these interactions with increasing efficiency for decreasing π -pulse spacing [52]. Thus, our findings that the reduction in the 29 Si FWHM of the echo train of Q 3 sites in the silicate glasses with increasing MAS and π -pulse train rates, as measured in this study, are consistent with previous work. At the fastest spinning speeds, the 29 Si FWHM values approach the values measured in the calcium silicate glass where relaxation is mainly mediated by the presence of paramagnetic impurities.

4.3. I couplings

The ability to measure J couplings accurately will require 29 Si MAS-PIETA FWHM values that are, ideally, an order of magnitude smaller than the J coupling, i.e., a FWHM of ~ 0.5 Hz, which is twice the width introduced by paramagnetic impurities. Based on the results of this study, it is possible to measure J coupling distributions using moderate MAS speeds in all alkali silicate glasses except the lithium silicates, where MAS speeds above $100 \, \text{kHz}$ would be needed to obtain a FWHM of $1.5 \, \text{Hz}$. Additionally, we note that the intercepts for the sodium and lithium silicate glasses in Table 6 would suggest FWHM lower limits of $\Lambda_{\text{MAS}} = 1.3 \, \text{Hz}$ and $\Lambda_{\text{MAS}} = 1.1 \, \text{Hz}$, respectively, highlighting the importance of avoiding paramagnetic impurities for an accurate determination of J couplings.

Finally, we turn our attention to the geminal ${}^2J_{\text{Si-O-Si}}$ couplings in Table 3, noting that there is a decrease by over a factor of two in the mean ${}^2J_{\text{Si-O-Si}}$ values in going from pure silica, i.e., all Q^4-Q^4 linkages, to the network modified silicate glasses, i.e., from 12.5 Hz to \sim 4 to 5 Hz. From first-principles DFT calculations on model disilicate clusters, Srivastava et al. [5] found that the geminal ${}^2J_{\text{Si-O-Si}}$ coupling across a ${}^{29}\text{Si-O-}{}^{29}\text{Si}$ linkage approximately follows

$$^{2}J_{\text{Si-O-Si}} \propto a_{\text{Si}_{i}}^{2}a_{\text{Si}_{j}}^{2}a_{\text{O}}^{4} = \left(a_{\text{Si}_{i}}^{2}a_{\text{O}}^{2}\right)\left(a_{\text{Si}_{j}}^{2}a_{\text{O}}^{2}\right),\tag{23}$$

where $(a_{\rm Si_i}^2 a_{\rm O}^2)$ and $(a_{\rm Si_j}^2 a_{\rm O}^2)$ are the products of the s-character of the valence hybrid-type orbitals (HTO) associated with the Si⁽ⁱ⁾–O and Si^(j)–O bonds across Si⁽ⁱ⁾–O-Si^(j) linkage, respectively.

In a Q^4 environment, the s-character of each of the four valence HTOs on silicon is 25% as all Si–O bonds have the same length. For silicon in a Q^3 environment, however, the Si–O bond with a non-bridging oxygen (NBO) is shorter than the other three Si–O bonds with bridging oxygens (BO) [19,39]. This shortening of the Si–NBO bond leads to a corresponding increase in its silicon HTO s-character above 25% and a correlated s-character decrease below 25% in the remaining three silicon HTOs involving the Si–BO—the sum of the four s-characters must remain 100%. Thus, the observed decrease in $^2J_{\text{Si-O-Si}}$ in the network-modified silicate glasses relative to silica glass is not surprising as this decrease in the s-character of the Si–BO HTO with the addition of each NBO in a Q^n environment leads to a decrease in the $^2J_{\text{Si-O-Si}}$ coupling through the Si–BO bonds as n decreases from 4.

It is noteworthy that the larger variance in the *J* coupling distributions of the alkaline earth silicate glasses is consistent with greater structural disorder from network modifier cations of high

cation potential. That is, the modifier cations Ca²⁺ and Ba²⁺ lead to an increase in the disproportionation reactions

$$2Q^{n} \rightleftharpoons Q^{n-1} + Q^{n+1},$$
 (24)

and

$$20^0 \rightleftharpoons 20^1 + 0^{2-},\tag{25}$$

in the melt from which the glass was formed and therefore more disorder is expected in the types of anionic species present in the glass [53–55,32,32,19].

5. Conclusions

We have found that the nuclear spin characteristics of modifier cations in silicate glasses play a significant role in determining ²⁹Si MAS-PIETA coherence lifetimes, causing orders of magnitude changes depending on the modifier cation identity. In glass compositions with abundant NMR active nuclei, such as the alkali silicate glasses, we show that the ²⁹Si MAS-PIETA coherence lifetime is dominated by coherent dephasing due to residual heteronuclear dipolar couplings. In this case, we observe a near-linear decrease in the residual broadenings with increasing MAS speed and π pulse train rate, although rf inhomogeneities often limit π -pulse trains as an effective averaging technique at the higher π -pulse train rates. With increasing MAS speeds the residual ²⁹Si heteronuclear dipolar couplings in the alkali silicate glasses are eventually removed, leaving the ²⁹Si MAS-PIETA coherence lifetimes limited by incoherent dephasing due to paramagnetic impurities. In glass compositions dilute in NMR active nuclei, such as the alkaline earth silicate glasses, the ²⁹Si MAS-PIETA coherence lifetimes are considerably longer and limited only by incoherent dephasing due to paramagnetic impurities. In this case, the coherence lifetimes are generally unaffected by increasing MAS speed beyond a low threshold speed of a few hundred hertz needed to remove homonuclear ²⁹Si-²⁹Si dipolar couplings. In all glass compositions in this study, any incoherent dephasing due to diffusive motion of network modifier cations or nuclear relaxation of alkali cations at room temperature is shown to be an inefficient ²⁹Si relaxation mechanism.

With sufficient reduction of residual heteronuclear dipolar couplings, the $^{29}\mathrm{Si}$ MAS-PIETA signal can be analyzed to obtain the $^2J_{\mathrm{Si-O-Si}}$ coupling distribution [2]. We measured the geminal $^2J_{\mathrm{Si-O-Si}}$ coupling distribution parameters in the sodium, potassium, calcium, and barium silicate glasses from the J-modulation of the $^{29}\mathrm{Si}$ PIETA signal. It was not possible to detect any J modulation in the lithium silicate glass due to its short $^{29}\mathrm{Si}$ coherence lifetime at the MAS rates (14 kHz) used in this study. Our results suggest, however, that it may be possible to measure geminal $^2J_{\mathrm{Si-O-Si}}$ couplings in lithium silicate glass at MAS speeds approaching 100 kHz.

In short, a combination of high-power rf pulses and fast magicangle spinning can eliminate residual heteronuclear dipolar couplings to other abundant NMR active nuclei, enabling (1) greater ²⁹Si NMR sensitivity enhancements in silicate glasses using CPMG and (2) more accurate measurements of ²⁹Si *J* couplings in network modified silicate glasses [15,2]. Conversely, differential ²⁹Si MAS-PIETA coherence lifetimes arising from residual heteronuclear dipolar couplings at slower MAS speeds can also serve as sensitive probes of variations in the local environment around silicon.

Data Availability Statement

The experimental CSDM-compliant [56] datasets that support the findings of this study are openly available in Zenodo at http://doi.org/10.5281/zenodo.5541736, reference number [57].

Declaration of Competing Interest

The authors declare that they have no known competing financial interests or personal relationships that could have appeared to influence the work reported in this paper.

Acknowledgements

The authors thank Matthias Ernst for helpful discussions. This material is based upon work supported by the Chemical Measurement and Imaging program in the National Science Foundation Division of Chemistry under Grant No. CHE-1807922 (with partial co-funding from the Ceramics program in the Division of Materials Research).

Appendix A. Supplementary material

Plots of the experimental ²⁹Si static and MAS spectra of all glass compositions in this study and tables of the experimental NMR acquisition parameters. Supplementary data associated with this article can be found, in the online version, at https://doi.org/10.1016/j.imr.2021.107097.

References

- D.J. Srivastava, P.J. Grandinetti, Statistical learning of NMR tensors from 2D isotropic/anisotropic correlation nuclear magnetic resonance spectra, J. Chem. Phys. 153 (2020) 134201, https://doi.org/10.1063/5.0023345.
- [2] D. Srivastava, J. Baltisberger, P. Florian, F. Fayon, R. Shakhovoy, M. Deschamps, N. Sadiki, P. Grandinetti, Correlating structural distributions in silica glass with two-dimensional j-resolved spectroscopy, Phys. Rev. B 9867 (2018), https://doi.org/10.1103/PhysRevB.98.134202. 134202-1-18.
- [3] N.M. Trease, T.M. Clark, P.J. Grandinetti, J.F. Stebbins, S. Sen, Bond length-bond angle correlation in densified silica-results from ¹⁷O NMR spectroscopy, J. Chem. Phys. 146 (2017) 184505, https://doi.org/10.1063/1.4983041.
- [4] M. Eden, NMR studies of oxide-based glasses, Annu. Rep. Prog. Chem., Sect. C: Phys. Chem. 108 (2012) 177–221, https://doi.org/10.1039/C2PC90006H.
- [5] D.J. Srivastava, P. Florian, J.H. Baltisberger, P.J. Grandinetti, Correlating geminal ²J_{Si-O-Si} couplings to structure in framework silicates, Phys. Chem. Chem. Phys. 20 (2018) 562–571, https://doi.org/10.1039/C7CP06486A.
- [6] J. Waugh, Sensitivity in Fourier transform NMR spectroscopy of slowly relaxing systems, J. Mol. Spectrosc. 35 (1970) 298–305, https://doi.org/10.1016/0022-2852(70)90205-5.
- [7] A. Allerhand, D.W. Cochran, Carbon-13 Fourier-transform nuclear magnetic resonance. i. Comparison of a simple spin-echo procedure with other methods, J. Am. Chem. Soc. 92 (1970) 4482–4484, https://doi.org/10.1021/ja00717a071.
- [8] N.M. Szeverenyi, A. Bax, G.E. Maciel, Magic-angle hopping as an alternative to magic-angle spinning for solid-state NMR, J. Magn. Reson. 61 (1985) 440, https://doi.org/10.1016/0022-2364(85)90184-2.
- [9] T. Vosegaard, F.H. Larsen, H.J. Jakobsen, P.D. Ellis, N.C. Nielsen, Sensitivity-enhanced multiple-quantum MAS NMR of half-integer quadrupolar nuclei, J. Am. Chem. Soc. 119 (38) (1997) 9055–9056, https://doi.org/10.1021/ja971355u.
- [10] D. Jardón-Álvarez, M.O. Bovee, J.H. Baltisberger, P.J. Grandinetti, Natural abundance ¹⁷O and ³³S nuclear magnetic resonance spectroscopy in solids achieved through extended coherence lifetimes, Phys. Rev. B 100 (2019), https://doi.org/10.1103/PhysRevB.100.140103, 140103-1-140103-5.
- [11] U. Haeberlen, J.S. Waugh, Spin-lattice relaxation in periodically perturbed systems, Phys. Rev. 185 (1969) 420–429, https://doi.org/10.1103/ PhysRev.185.420.
- [12] M.M. Maricq, J.S. Waugh, NMR in rotating solids, J. Chem. Phys. 70 (1979) 3300, https://doi.org/10.1063/1.437915.
- [13] P. Schanda, M. Ernst, Studying dynamics by magic-angle spinning solid-state NMR spectroscopy: Principles and applications to biomolecules, Prog. NMR Spect. 96 (2016) 1–46, https://doi.org/10.1016/j.pnmrs.2016.02.001.
- [14] A.J. Vega, Relaxation in spin-echo and spin-lock experiments, J. Magn. Reson. 65 (1985) 252–267, https://doi.org/10.1016/0022-2364(85)90006-X.
- [15] P. Florian, F. Fayon, D. Massiot, ⁽²⁾ Si-O-Si scalar spin-spin coupling in the solid state: Crystalline and glassy wollastonite CaSiO₃, J. Phys. Chem. C 113 (2009) 2562–2572, https://doi.org/10.1021/jp8078309.
- [16] J.H. Baltisberger, B.J. Walder, E.G. Keeler, D.C. Kaseman, K.J. Sanders, P.J. Grandinetti, Phase incremented echo train acquisition in NMR spectroscopy, J. Chem. Phys. 136 (2012), https://doi.org/10.1063/1.4728105, 211104-1-4.
- [17] E.A. Porai-Koshits, Genesis of concepts on structure of inorganic glasses, J. Non-Cryst. Solids 123 (1990) 1–13, https://doi.org/10.1016/0022-3093(90) 90767-G.

- [18] A. Wright, Neutron scattering from vitreous silica. V. the structure of vitreous silica: What have we learned from 60 years of diffraction studies?, J Non Cryst. Solids 179 (1994) 84–115, https://doi.org/10.1016/0022-3093(94)90687-4.
- [19] J.H. Baltisberger, P. Florian, E.G. Keeler, P.A. Phyo, K.J. Sanders, P.J. Grandinetti, Modifier cation effects on ²⁹Si nuclear shielding anisotropies in silicate glasses, J. Magn. Reson. 268 (2016) 95–106, https://doi.org/10.1016/j.jmr.2016.05.003.
- [20] J.L. Markley, W.J. Horsley, M.P. Klein, Spin-lattice relaxation measurements in slowly relaxing complex spectra, J. Chem. Phys. 55 (1971) 3604–3605, https:// doi.org/10.1063/1.1676626.
- [21] A. Lesage, M. Bardet, L. Emsley, Through-bond carbon-carbon connectivities in disordered solids by NMR, J. Am. Chem. Soc. 121 (1999) 10987–10993, https:// doi.org/10.1021/ja992272b.
- [22] N. Bloembergen, E.M. Purcell, R.V. Pound, Relaxation effects in nuclear magnetic resonance absorption, Phys. Rev. 73 (1948) 679–712, https://doi. org/10.1103/PhysRev.73.679.
- [23] E.L. Hahn, Spin echoes, Phys. Rev. 80 (4) (1950) 580-594.
- [24] A. Abragam, Principles of Nuclear Magnetism, Oxford University Press, Oxford, 1961.
- [25] R.R. Ernst, G. Bodenhausen, A. Wokaun, Principles of Nuclear Magnetic Resonance in One and Two Dimensions, Oxford University Press, Oxford, 1987.
- [26] P.J. Grandinetti, J.T. Ash, N.M. Trease, Symmetry pathways in solid-state NMR, Prog. Nucl. Mag. Res. Sp. 59 (2011) 121–196, https://doi.org/10.1016/j. pnmrs.2010.11.003.
- [27] A. Allerhand, Analysis of carr-purcell spin-echo nmr experiments on multiplespin systems. i. the effect of homonuclear coupling, J. Chem. Phys. 44 (1966) 1, https://doi.org/10.1063/1.1726430.
- [28] R. Freeman, H.D.W. Hill, High-resolution study of NMR spin echoes: "J Spectra", J. Chem. Phys. 54 (1971) 301–313, https://doi.org/10.1063/ 1.1674608.
- [29] L. Duma, W.C. Lai, M. Carravetta, L. Emsley, S.P. Brown, M.H. Levitt, Principles of spin-echo modulation by J-couplings in magic-angle-spinning solid-state NMR, Chem. Phys. Chem. 5 (6) (2004) 815–833, https://doi.org/10.1002/ cphc.200301213.
- [30] E.L. Hahn, D.E. Maxwell, Spin echo measurements of nuclear spin coupling in molecules, Phys. Rev. 88 (1952) 1070–1084, https://doi.org/10.1103/ PhysRev.88.1070.
- [31] M. Davis, D.C. Kaseman, S.M. Parvani, K.J. Sanders, P.J. Grandinetti, P. Florian, D. Massiot, Q⁽ⁿ⁾-species distribution in K₂O 2SiO₂ by ²⁹Si Magic Angle Flipping NMR, J. Phys. Chem. A 114 (17) (2010) 5503–5508, https://doi.org/10.1021/jp100530m.
- [32] M. Davis, K.J. Sanders, P.J. Grandinetti, S.J. Gaudio, S. Sen, Structural investigations of magnesium silicate glasses by ²⁹Si magic-angle flipping NMR, J. Non. Cryst. Solids 357 (2011) 2787–2795, https://doi.org/10.1016/j. jnoncrysol.2011.02.045.
- [33] R.D. Shannon, C.T. Prewitt, Effective ionic radii in oxides and fluorides, Acta Cryst B 25 (1969) 925–946, https://doi.org/10.1107/S0567740869003220.
- [34] N.P. Bansal, R.H. Doremus, Handbook of Glass Properties, Elsevier, Orlando, Florida, 1986. doi:10.1016/C2009-0-21785-5.
- [35] R. Terai, R. Hayami, Ionic diffusion in glasses, J. Non-Cryst. Solids 18 (1975) 217–264, https://doi.org/10.1016/0022-3093(75)90022-8.
- [36] E. Göble, W. Müller-Warmuth, H. Olyschläger, H. Dutz, ⁷Li NMR spectra, nuclear relaxation, and lithium ion motion in alkali silicate, borate, and phosphate glasses, J. Magn. Reson. 36 (1979) 371–387, https://doi.org/10.1016/0022-2364(79)90114-8.
- [37] R. Zallen, The Physics of Amorphous Solids, Wiley, New York, 1983.
- [38] G.N. Greaves, EXAFS and the structure of glass, J. Non-Cryst. Solids 71 (1985) 203–217, https://doi.org/10.1016/0022-3093(85)90289-3.
- [39] D. Jardón-Álvarez, K.J. Sanders, P. Phyo, J.H. Baltisberger, P.J. Grandinetti, Cluster formation of network-modifier cations in cesium silicate glasses, J. Chem. Phys. 148 (2018) 094502, https://doi.org/10.1063/1.5020986.

- [40] A. George, J. Stebbins, Dynamics of Na in sodium aluminosilicate glasses and liquids, Phys. Chem. Miner. 23 (1996) 526–534, https://doi.org/10.1007/ BF00242002.
- [41] S. Sen, A. George, J. Stebbins, Ionic conduction and mixed cation effect in silicate glasses and liquids: ²³Na and ⁷Li NMR spin-lattice relaxation and a multiple-barrier model of percolation, J. Non-Cryst. Solids 197 (1996) 53–64, https://doi.org/10.1016/0022-3093(95)00615-X.
- [42] P. Mansfield, Symmetrized pulse sequences in high resolution nmr in solids, J. Phys. C 4 (1971) 1444–1452, https://doi.org/10.1088/0022-3719/4/11/020.
- [43] M. Mehring, High Resolution NMR Spectroscopy in Solids, vol. 11, Springer-Verlag, Berlin, 1983.
- [44] D. Li, Y. Dong, R.G. Ramos, J.D. Murray, K. MacLean, A.E. Dementyev, S.E. Barrett, Intrinsic origin of spin echoes in dipolar solids generated by strong, Phys. Rev. B 77 (2008), https://doi.org/10.1103/PhysRevB.77.214306.
- [45] M. Mehring, G. Sinning, A. Pines, NMR line broadening in solids by slowing down of spin fluctuations, Z. Physik B 24 (1976) 73–76, https://doi.org/ 10.1007/BF01312875.
- [46] M. Ernst, A. Verhoeven, B.H. Meier, High-speed magic-angle spinning ¹³C MAS NMR spectra of adamantane: Self-decoupling of the heteronuclear scalar interaction and proton spin diffusion, J. Magn. Reson. 130 (1998) 176–185, https://doi.org/10.1006/jmre.1997.1311.
- [47] H. Kessemeier, R.E. Norberg, Pulsed nuclear magnetic resonance in rotating solids, Phys. Rev. 155 (1967) 321–337, https://doi.org/10.1103/ PhysRev.155.321.
- [48] V.E. Zorin, S.P. Brown, P. Hodgkinson, Origins of linewidth in ¹H magic-angle spinning NMR, J. Chem. Phys. 125 (2006) 144508, https://doi.org/10.1063/ 1.2357602.
- [49] U. Sternberg, R. Witter, I. Kuprov, J.M. Lamley, A. Oss, J.R. Lewandowski, A. Samoson, ¹H line width dependence on MAS speed in solid state NMR comparison of experiment and simulation, J. Magn. Reson. 291 (2018) 32–39, https://doi.org/10.1016/j.jmr.2018.04.003.
- [50] T.D. Ladd, D. Maryenko, Y. Yamamoto, E. Abe, K.M. Itoh, Coherence time of decoupled nuclear spins in silicon, Phys. Rev. B 71 (2005) 014401, https://doi. org/10.1103/PhysRevB.71.014401.
- [51] S.R. Chaudhari, P. Berruyer, D. Gajan, C. Reiter, F. Engelke, D.L. Silverio, C. Copéret, M. Lelli, A. Lesage, L. Emsley, Dynamic nuclear polarization at 40 kHz magic angle spinning, PCCP 18 (2016) 10616–10622, https://doi.org/10.1039/ C6CP008394
- [52] G.A. Álvarez, A. Ajoy, X. Peng, D. Suter, Performance comparison of dynamical decoupling sequences for a qubit in a rapidly fluctuating spin bath, Phys. Rev. A 82 (2010). doi: 10.1103/PhysRevA.82.042306.
- [53] J.B. Murdoch, J.F. Stebbins, I.S.E. Carmichael, High-resolution ²⁹Si NMR study of silicate and aluminosilicate glasses: the effect of network-modifying cations, Am. Mineral. 70 (1985) 332–343.
- [54] G. Libourel, C.A. Gieger, L. Merwin, A. Sebald, ²⁹Si and ²⁷Al MAS-NMR spectroscopy of glasses in the system CaSiO₃-MgSiO₃-Al₂O₃, Chem. Geol. 96 (1992) 387–397.
- [55] P. Zhang, P.J. Grandinetti, J.F. Stebbins, Anionic species determination in CaSiO₃ glass using two-dimensional ²⁹Si NMR, J. Phys. Chem. B 101 (20) (1997) 4004–4008, https://doi.org/10.1021/jp9700342.
- [56] D.J. Srivastava, T. Vosegaard, D. Massiot, P.J. Grandinetti, Core scientific dataset model: A lightweight and portable model and file format for multidimensional scientific data, PLoS ONE 15 (2020), doi:10.1371/journal. pone.0225953.
- [57] D. Jardón-Álvarez, M.O. Bovee, P.J. Grandinetti, Silicon-29 nmr experimental datasets used in silicon-29 echo train coherence lifetimes and geminal jcouplings in network modified silicate glasses (2021). doi:10.5281/ zenodo.5541736. doi: 10.5281/zenodo.5541736.